Asian Journal of Chemistry; Vol. 25, No. 7 (2013), 3633-3643

ASIAN JOURNAL OF CHEMISTRY

http://dx.doi.org/10.14233/ajchem.2013.13690

DFT Study of the Effect of Different Metals on Structures and Electronic Spectra of Some Organic-Metal Compounds as Sensitizing Dyes

GUODONG TANG[1,2,*], RONGQING LI[2], SHANSHAN KOU[2,3], HU ZHOU[2,4], YU ZHANG[2], XUEHAI JU[1] and CHANGMEI WEI[2]

[1]School of Chemical Engineering, Nanjing University of Science and Technology, Nanjing 210094, P.R. China
[2]Jiangsu Key Laboratory for Chemistry of Low-Dimensional Materials, School of Chemistry and Chemical Engineering, Huaiyin Normal University, Huai'an 223300, Jiangsu Province, P.R. China
[3]School of Chemistry & Chemical Engineering, Ningxia University, Yinchuan 750021, P.R. China
[4]College of Chemistry and Chemical Engineering, Nanjing University of Technology, Nanjing 210009, P.R. China

*Corresponding author: Fax: +86 517 83525320; Tel: +86 517 83525318; E-mail: hysytanggd@hotmail.com

(*Received*: 7 March 2012; *Accepted*: 7 January 2013) AJC-12665

Ruthenium polypyridine-derivative complexes are used in dye-sensitized solar cell (DSSC) as a light to current conversion sensitizer. In order to lower cost of the dye-sensitized solar cell, the normal transition metals were used to replace the noble metal ruthenium and some compounds [ML_2] (M = Ru, Ni, Mn, Cu; L = 5'-methyl-2, 2'-bipyridine-6-carboxylato, **I** = RuL_2, II = NiL_2, **III** = MnL_2, **IV** = CuL_2) were selected as the replacement. The geometries, electronic structures and optical absorption spectra of these compounds have been studied by using density functional theory (DFT) calculation at the B3P86/LANL2DZ level of theory. The maximum absorptions of complexes are found to be at 646 and 979 nm for compound **III** and 617 nm for compound **IV**. The λ_{max} band in complexes **III** and **IV** have a large red-shift when compared to the standard compound **I**. This means that the panchromatic response of compounds **III** and **IV** renders it as a suitable sensitizer for solar energy conversion applications.

Key Words: DFT, Different metals, Organic-metal compounds, Sensitizing dyes.

INTRODUCTION

The new types of dye sensitized solar cells (DSSCs) have attracted a considerable amount of interest since Grätzel and co-workers[1-4] reported that the photoelectricity conversion efficiency was obtained to be more than 7.1 % and they offer the possibility of low-cost conversion of photovoltaic energy. To increase the photoconversion efficiency, different approaches are still being studied to improve the photoelectricity conversion efficiency of the dye-sensitized solar cell, such as the nature of semiconductors (TiO_2, SnO_2, ZnO, NiO, *etc.*)[5-8], the morphology of semiconductors (TiO_2, ZnO *etc.*)[9-11] and the forms of electrolytes[12,13]. In the cells, the sensitizer is one of the key components, harvesting the solar radiation and converting it to electric current.

It has been found that many organic-metal compounds possess promising high conversion efficiency since these kinds of organic-metal compounds were found to combine the advantages of molecular tunability with the material properties of wide band-gap semiconductors, such as stability toward corrosion, charge transport and mechanical resilience. Until now, many efforts have been done on the syntheses of new ruthenium complexes and determinations of their electronic spectra[14-20] and state-of-the-art dye-sensitized solar cells based on ruthenium(II)-polypyridyl complexes as the active material have an overall power conversion efficiency (η) approaching 11 % under standard (Global Air Mass 1.5) illumination[21-24]. The ruthenium polypyridine and polypyridine-derivative complexes have been widely investigated for many years both experimentally and theoretically. Komatsuzaki and co-workers[25] synthesized a series of ruthenium (II)-polypyridyl complexes as a sensitizer for dye-sensitized solar cell and characterized their photophysical and photochemical properties; the complexes showed broad electronic absorption bands in the near-IR region. Xu and co-workers[26] reported the behaviours of RuL_2 (L = 5'-methyl-2, 2'-bipyridine-6-carboxyl) in the gas phase and DMF solution by the TD-DFT method. Their calculation results indicate that the two maximum absorption peaks are blue-shifted in DMF solution in comparison with those in the gas phase. Nazeeruddin[27] and co-workers reported a ruthenium complex *trans*-[Ru(L')$(NCS)_2$], where L' = 4,4'''-di-*tert*-butyl-4', 4''-*bis*(carboxylic acid)-2, 2':6', 2'':6'', 2''' quaterpyridine (N886) and the complex was characterized by spectroscopic and electrochemical methods. The electronic

spectrum of the N886 complex was also calculated by TD-DFT method. The result showed its absorption bands as mixed Ru/SCN-to-quarterpyridine charge-transfer transitions, which extend from the near-IR to the UV regions. This suggests that it can act as a suitable sensitizer for solar energy conversion applications. These studies put the attention mainly on the effect of the different ligands on the dye-sensitized solar cells properties. However, ruthenium is a noble metal and it may be a bottleneck for the development of the low-cost dye-sensitized solar cells. At present, little attentions have been paid to the normal transition metals and their effect on the dye-sensitized solar cells.

In order to reduce the cost of the dye-sensitized solar cells, we wish to use the normal transition metals to replace the noble metal. We selected a reported ruthenium polypyridine-derivative complex[26,28] as an object of reference and the different transition metals were used to replace the ruthenium. In order to understand the relationship between the metals and the dye-sensitized solar cells properties, the DFT methods were used to optimize the structures of those organic metals without any constrains in bond lengths, bond angles and dihedral angles and then calculated the electronic spectra of those optimized structures. The results would be helpful in the simulation, screening and design of new organic metal complexes as new dye-sensitized solar cells sensitizers.

COMPUTATIONAL METHOD

Due to the high accuracy, DFT has been proved to be more useful in calculating molecular properties of the organo-metallic compounds than the traditional *ab initio* electronic structure methods[29,30]. Some reports indicated that the ruthenium polypyridine-derivative complexes are efficient photosensitizers because of their broad range of visible light absorption and relatively long lived excited states, with energies almost matching those of TiO_2 conduction band states[31-34].

The geometries of these complexes were optimized using the DFT (B3LYP and B3P86) methods and the LANL2DZ or LANL2MB basis set[35-40]. The UV-visible spectra of these complexes were calculated with the same method. Geometry optimization is one of the most important steps in the theoretical calculations. This procedure proceeds in two steps. Firstly the geometry was constructed by MM + molecular dynamics in Hyper-Chem. 7.0 Package[41] and then optimized by the DFT methods at B3LYP or B3P86 level with LanL2DZ or LANL2MB basis set using Gaussian 03W program package. The maximum values of the converged criterion are default. All geometries converged perfectly. The HOMO-LUMO gap was computed at the same theoretical level as that used in the geometry optimization. Meanwhile, the time-dependent density functional theory (TD-DFT) was employed to describe the electron absorption spectra of all organic metals.

RESULTS AND DISCUSSION

Structures: Any comparison between experimental and calculated data should require a precise knowledge of the molecular structure of the complexes. However, only a few crystal structures of these organic-metal complexes have been reported to date. We selected these reported crystal structure as comparison.

The fully optimized geometries of $[ML_2]$ (M = Ru, Ni, Mn, Cu; L = 5'-methyl-2, 2'-bipyridine-6-carboxylato) are shown in Fig. 1. The selected bond lengths and bond angles are given in Table-1, along with the available experimental data[28].

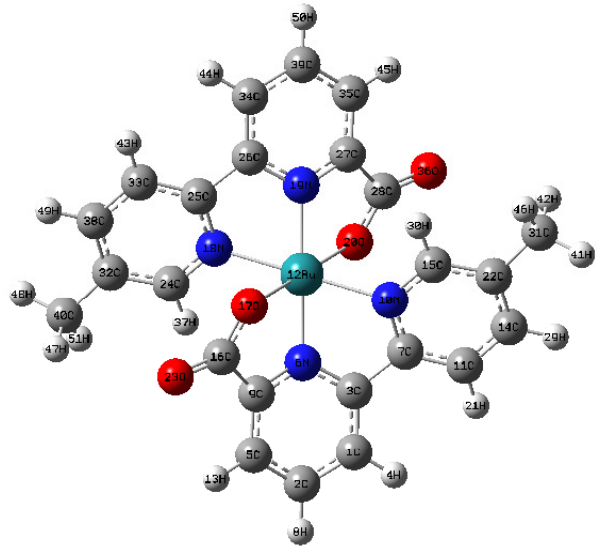

I

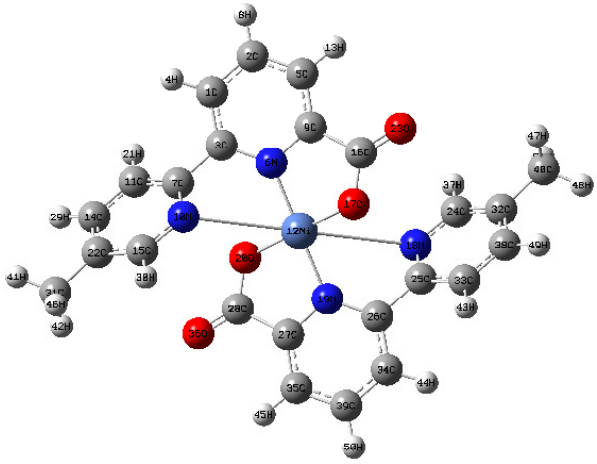

II

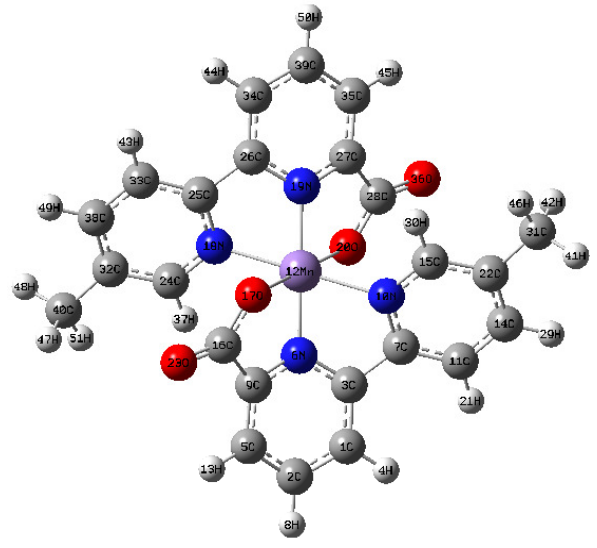

III

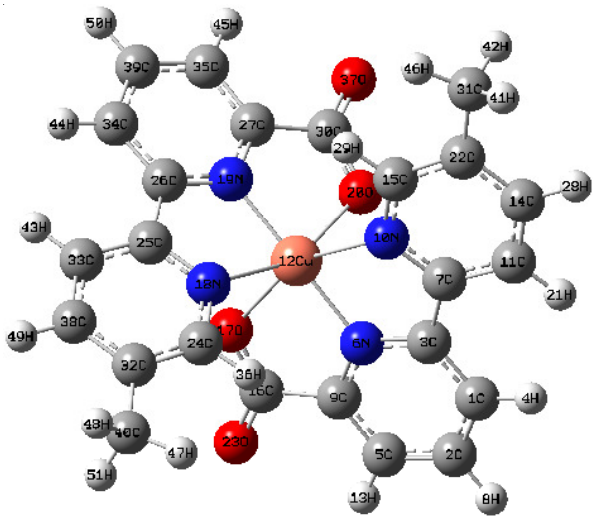

IV

Fig. 1. Optimized geometries of ML_2 complex. (M = Ru, Ni, Mn, Cu, L = 5'-methyl-2, 2'-bipyridine-6-carboxylato), **I** = RuL_2, **II** = NiL_2, **III** = MnL_2, **IV** = CuL_2)

In order to evaluate the method exactness, we selected the reported structure[28] for comparison. The relative errors for different methods (B3LYP/LANL2DZ, B3LYP/LANL2MB, B3P86/ LANL2DZ and B3P86/ LANL2MB) were in the range of 2.3-5.3, 1.6-4.3, 0.9-3.5 and 1.7-3.0 % for bond lengths and 4.8-7.0, 4.4-6.4, 4.6-6.6 and 4.2-6.1 % for bond angles, respectively. These geometric parameters are close to the experimental values, suggesting that these methods were appropriate for these types of compounds. Since the exact crystal structures of the other title compounds are not available till now, the optimized structures can only be compared with other similar systems for which the crystal structures have been reported[42-46]. The Cu-N bond length ranges in the literature are 1.952-2.006 Å[42,43], while the calculated values with different methods (B3LYP/LANL2DZ, B3LYP/LANL2MB, B3P86/ LANL2DZ and B3P86/LANL2MB) are 1.981-2.361, 2.094-2.354, 1.960-2.313, 2.037-2.426 Å, respectively. The Mn-N bond length ranges in the literature are 2.252-2.282 Å[44,45], while the calculated values with different methods (B3LYP/ LANL2DZ, B3LYP/LANL2MB, B3P86/LANL2DZ and B3P86/LANL2MB) are 1.948-2.131, 1.914-2.063, 1.915-2.066, 1.892-2.031 Å, respectively. The Ni-N bond length ranges are 2.064-2.084 Å[46], while the calculated values with different methods (B3LYP/LANL2DZ, B3LYP/LANL2MB, B3P86/LANL2DZ and B3P86/LANL2MB) are 1.948, 1.934, 1.921, 1.911Å, respectively. The Cu-O bond length ranges are 1.935-1.944 Å[42,43], while the calculated values with different methods (B3LYP/LANL2DZ, B3LYP/LANL2MB, B3P86/ LANL2DZ and B3P86/LANL2MB) are 2.106-2.107, 2.012-2.069, 2.099-2.099, 2.125-2.125 Å, respectively. The Mn-O bond length ranges are 2.104-2.104 Å[44,45], while the calculated values with different methods (B3LYP/LANL2DZ, B3LYP/ LANL2MB, B3P86/LANL2DZ and B3P86/ LANL2MB) are 2.059, 1.891, 2.022, 1.878 Å, respectively. The Ni-O bond length ranges are 2.055 Å[46], while the calculated values with different methods (B3LYP/LANL2DZ, B3LYP/LANL2MB, B3P86/LANL2DZ and B3P86/ LANL2MB) are 1.870, 1.829, 1.856, 1.820 Å, respectively. From the theoretical values we can find that all the geometric parameters are close to the experimental values except a Ni-N bond length and the distances between the M-N(O) (M = Ru, Cu, Mn, Ni) atoms are slightly smaller than that sum of the M atom and N(O) atom radius. This means that there is a bond between the M atom and the nearest N (O) atom. These geometric parameters are close to the experimental values although the errors of the B3LYP/LANL2MB method were larger than those obtained from the other methods; the errors are in acceptable range. The other O atom from the carboxyl group can not connect the M atom and this may be as a suitable sensitizer for solar energy conversion applications based on the semiconductor (TiO_2, SnO_2, ZnO, NiO, *etc.*) mesoporous electrodes. The same methods were used to calculate the IR spectra of these compounds. The outcome shows that the structures of these compounds are stable as there is not any imaginary vibration model. The other properties were calculated base on these structures.

Electronic structure: Results for the electronic structure of these complexes were schematized in the molecular orbital energy diagram of Fig. 2. The local densities of states of compounds were listed in Table-2. The isodensity plots of selected frontier orbital's for M(II) L_2 (M = Ru, Ni, Mn, Cu) were shown in Fig. 3.

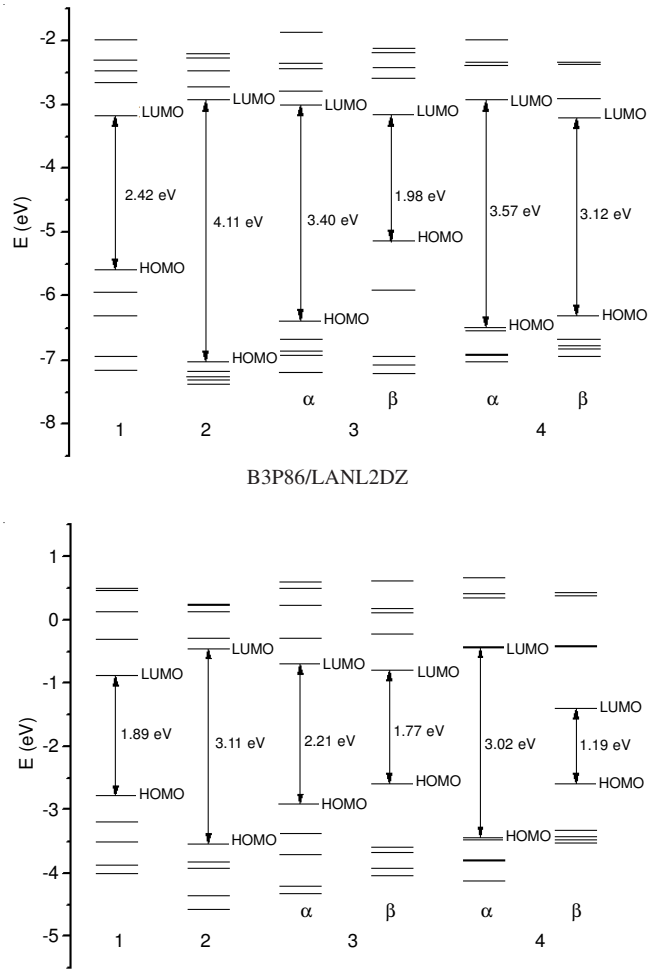

1. $Ru(II)L_2$, 2. $Ni(II)L_2$, 3. $Mn(II)L_2$, 4. $Cu(II)L_2$

Fig. 2. Energy levels (eV) of the complexes base on the B3P86/LANL2DZ and the B3P86/LANL2MB

TABLE-1
SELECT BOND LENGTH (Å) AND BOND ANGLES (°) FOR ALL COMPOUNDS

Compounds	Parameters	B3LYP		B3P86		Exp.[28]
		Lanl2dz	Lanl2mb	Lanl2dz	Lanl2mb	
I	Ru12-N6	2.033	2.030	2.009	2.010	1.975
	Ru12-N10	2.140	2.119	2.104	2.093	2.042
	Ru12-N18	2.140	2.119	2.103	2.093	2.032
	Ru12-N19	2.033	2.030	2.009	2.010	1.976
	Ru12-O17	2.175	2.091	2.146	2.076	2.126
	Ru12-O20	2.175	2.091	2.146	2.076	2.127
	N18-Ru12-N19	73.8	74.4	74.3	74.6	79.4
	N10-Ru12-N6	73.8	74.4	74.3	74.6	79.5
	N6-Ru12-N19	180.0	180.0	180.0	180.0	178.8
	N10-Ru12-N19	106.0	105.6	105.7	105.4	101.1
	N18-Ru12-N6	106.0	105.6	105.7	105.4	99.6
II	Ni12-N6	1.948	1.934	1.921	1.911	2.064[46]
	Ni12-N19	1.948	1.934	1.921	1.911	2.074
	Ni12-O17	1.870	1.829	1.856	1.820	2.055
	Ni12-O20	1.870	1.829	1.856	1.820	2.055
	N18-Ni12-N19	58.9	61.6	59.6	61.8	–
	N18-Ni12-N10	179.9	180.0	180.0	180.0	–
	N10-Ni12-N6	59.0	61.6	59.6	61.8	–
	N6-Ni12-N19	180.0	180.0	180.0	180.0	–
	N10-Ni12-N19	121.0	118.4	120.4	118.2	–
	N18-Ni12-N6	121.1	118.4	120.4	118.2	–
III	Mn12-N6	1.948	1.914	1.915	1.892	2.252[44,45]
	Mn12-N10	2.131	2.063	2.066	2.031	2.258
	Mn12-N18	2.131	2.063	2.066	2.031	2.282
	Mn12-N19	1.948	1.914	1.915	1.892	2.282
	Mn12-O17	2.059	1.891	2.022	1.878	2.104
	Mn12-O20	2.059	1.891	2.022	1.878	2.104
	N18-Mn12-N19	74.9	76.5	75.9	76.9	72.7
	N18-Mn12-N10	180.0	180.0	180.0	180.0	162.4
	N10-Mn12-N6	74.9	76.5	75.9	76.9	71.7
	N6-Mn12-N19	180.0	180.0	180.0	180.0	162.4
	N10-Mn12-N19	105.1	103.4	104.1	103.1	98.8
	N18-Mn12-N6	105.1	103.4	104.1	103.1	94.3
IV	Cu12-N6	1.981	2.222	1.960	2.037	1.952[42,43]
	Cu12-N18	2.361	2.325	2.313	2.426	1.999
	Cu12-N19	1.981	2.094	1.960	2.037	2.006
	Cu12-O17	2.107	2.012	2.099	2.125	1.9440
	Cu12-O20	2.106	2.069	2.099	2.125	2.305
	O17-Cu12-N6	80.5	79.1	80.6	79.0	91.0
	O18-Cu12-N6	110.3	110.3	110.1	116.0	165.4
	N6-Cu12-N19	172.4	155.3	171.9	167.5	166.7
	N6-Cu12-N20	95.6	95.6	95.0	94.4	93.0
	O17-Cu12-N18	81.0	98.7	80.8	83.4	85.0
	O17-Cu12-N19	95.1	125.2	95.0	94.4	91.3
	N18-Cu12-N19	74.9	73.5	75.7	73.2	81.1
	N18-Cu12-N20	151.8	153.1	152.9	146.9	–
	N19-Cu12-N20	80.5	79.9	80.6	79.0	84.0

In Fig. 2, based on the B3P86/LANL2DZ and B3P86/LANL2MB methods, we can see that the DEH-L values of compound **I** are 2.42 and 1.89 eV, respectively. The DEH-L values of compound **II** are 3.11 and 4.11 eV, which are larger than those of compound **I**. This means that compound **II** is not suitable as a sensitizer for solar energy conversion applications. For compounds **III** and **IV**, there are more electrons, thus the forms of electron transition are complex. The $\Delta E_{H\text{-}L}$ values of compound **III** are 3.40/2.21 for α electron, 1.98/1.77 for β electron and the $\Delta E_{H\text{-}L}$ values of compound **IV** are 3.57/3.02 for α electron, 3.12/1.19 for β electron, respectively. These values are close to those of compound **I**, meaning that compounds **III** and **IV** may be used as sensitizers for solar energy conversion applications.

As shown in Table-2 and Fig. 3, for compound **I** $Ru(II)L_2$, the HOMO (133), HOMO-1, HOMO-2 are a set of quasi-degenerated orbital's. Their largest orbital contributions derive from the metal atom (raging from 76-90 %) mixed with fewer characters of bipyridine rings and carboxylic groups (raging from 2-8 %). The HOMO-3 and HOMO-4 are mainly on the carboxylic groups (raging from 38-46 %). The five lowest LUMOs (134, 135, 136, 137 and 138) are almost entirely localized on the bipyridine rings (raging from 43-49 %), with only 1-7 % contribution from metal orbital. The tendencies

TABLE-2
ENERGIES AND PERCENTAGE COMPOSITION OF THE LOWEST UNOCCUPIED AND HIGHEST OCCUPIED ORBITALS OF THE COMPLEX IN TERMS OF Ru, BIPYRIDINE RINGS AND CARBOXYLIC FRAGMENTS

MO	occ	E (eV)	**I**	Bipyridine rings		Carboxylic groups	
				Ring 1a	Ring 2b	Group 1c	Group 2d
129	2	-5.75	18	3	3	38	38
130	2	-5.41	2	2	3	46	46
131	2	-4.74	90	2	2	3	3
132	2	-4.03	80	2	2	8	8
133	2	-3.46	76	8	8	3	3
134	0	3.96	1	5	48	1	1
135	0	4.53	7	46	46	0	0
136	0	5.34	1	48	45	4	4
137	0	5.68	5	43	35	5	5
138	0	5.80	1	49	49	1	1
MO	occ	E (eV)	**II**	Bipyridine rings		Carboxylic groups	
				Ring 1a	Ring 2b	Group 1c	Group 2d
121	2	-7.43	3	32	27	19	15
122	2	-7.06	2	37	37	11	10
123	2	-6.68	2	18	15	30	32
124	2	-6.11	7	1	1	46	45
125	2	-1.01	72	8	7	6	7
126	0	4.20	16	29	45	5	5
127	0	4.89	1	54	40	2	2
128	0	5.44	0	0	90	0	9
129	0	5.56	0	89	1	6	0
130	0	6.72	4	63	31	1	1
MO	occ	E (eV)	**III(α)**	Bipyridine rings		Carboxylic groups	
				Ring 1a	Ring 2b	Group 1c	Group 2d
120	2	-7.16	1	11	12	36	39
121	2	-7.07	1	42	39	9	9
122	2	-6.84	0	45	48	3	2
123	2	-6.24	1	1	4	4	39
124	2	-6.24	1	11	9	32	48
125	0	4.69	1	50	42	1	1
126	0	4.76	1	36	55	0	0
127	0	5.48	2	51	4	7	4
128	0	5.50	1	36	51	4	7
129	0	5.90	1	49	40	1	1
MO	occ	E (eV)	**III(β)**	Bipyridine rings		Carboxylic groups	
				Ring 1a	Ring 2b	Group 1c	Group 2d
120	2	-7.08	0	46	46	2	2
121	2	-6.14	3	1	1	48	47
122	2	-6.10	1	8	8	41	42
123	2	-0.656	12	48	47	1	1
124	2	2.089	1	48	41	1	1
125	0	5.02	0	55	39	2	1
126	0	5.06	1	38	55	2	3
127	0	5.69	0	47	45	3	3
128	0	5.90	1	47	41	2	2
129	0	6.99	1	44	43	5	5
MO	occ	E (eV)	**IV(α)**	Bipyridine rings		Carboxylic groups	
				Ring 1a	Ring 2b	Group 1c	Group 2d
122	2	-7.19	1	7	62	10	43
123	2	-7.15	1	7	25	23	14
124	2	-7.00	0	8	8	7	1
125	2	-6.31	1	8	2	84	3
126	2	-6.15	0	7	5	7	87
127	0	4.68	2	3	93	1	0
128	0	4.85	2	92	3	0	1
129	0	5.43	3	25	59	11	9
130	0	5.52	1	58	29	24	3
131	0	5.86	1	6	92	2	0

MO	occ	E (eV)	IV(β)	Bipyridine rings		Carboxylic groups	
				Ring 1a	Ring 2b	Group 1c	Group 2d
121	2	-7.29	1	4	18	18	59
122	2	-7.18	1	17	5	60	16
123	2	-6.38	1	2	4	6	88
124	2	-6.23	0	5	1	88	7
125	2	-0.31	1	51	45	1	1
126	0	2.18	1	46	51	1	1
127	0	5.07	3	24	66	2	5
128	0	5.31	0	67	25	5	2
129	0	5.79	1	12	83	1	2
130	0	5.95	1	84	12	3	1

[1a]Atoms N18, C24, C25, C26, C27, C32, C33, C34, C35, C38, C39 and N19 form ring 1. [2b]Atoms N6, C1, C2, C3, C5, C7, C9, C11, C14, C15, C22 and N10 form ring 2. [1c]AtomsO20, C28 and O36 form group 1. [2d]AtomsO17, C16 and O23 form group 2.

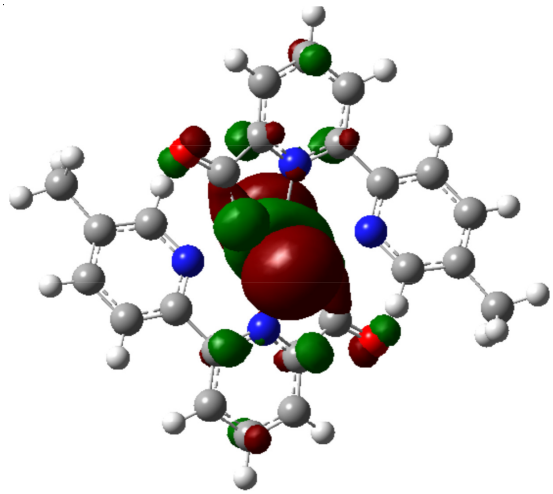

I-HOMO

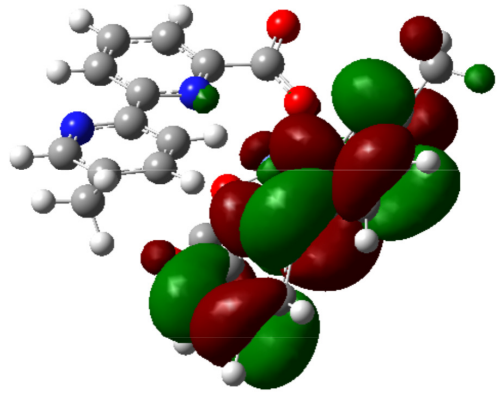

II-LUMO

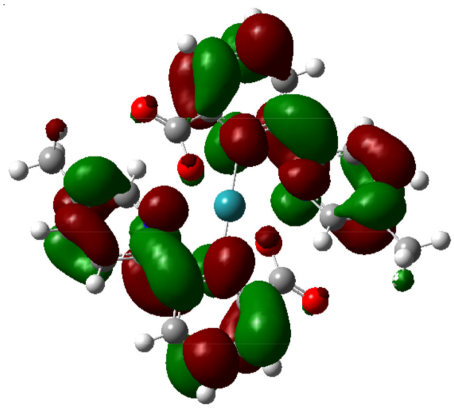

I-LUMO

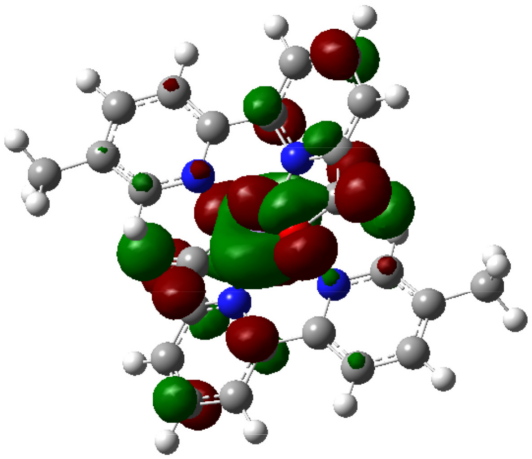

III-HOMO

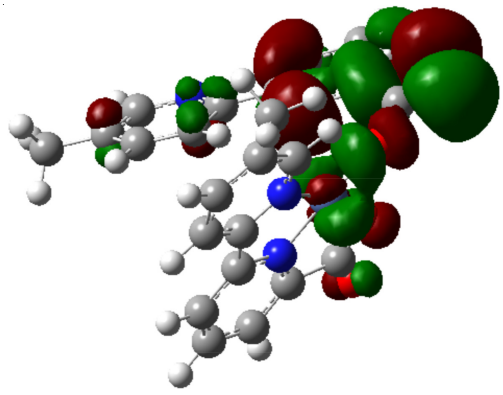

II-HOMO

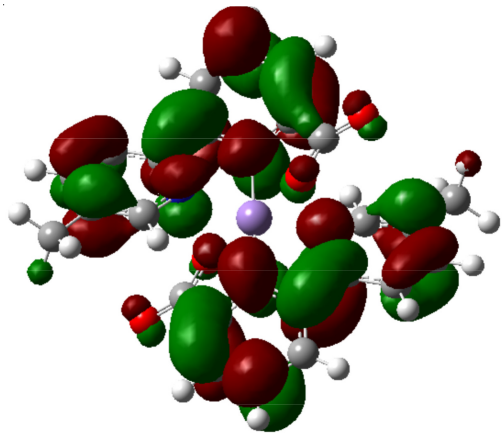

III-LUMO

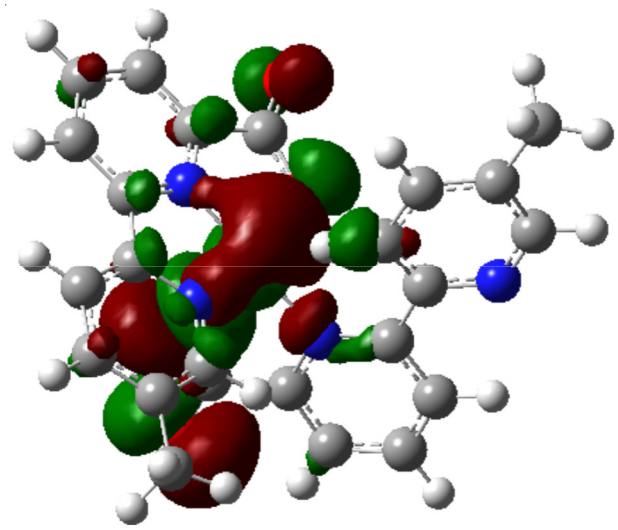

IV-HOMO

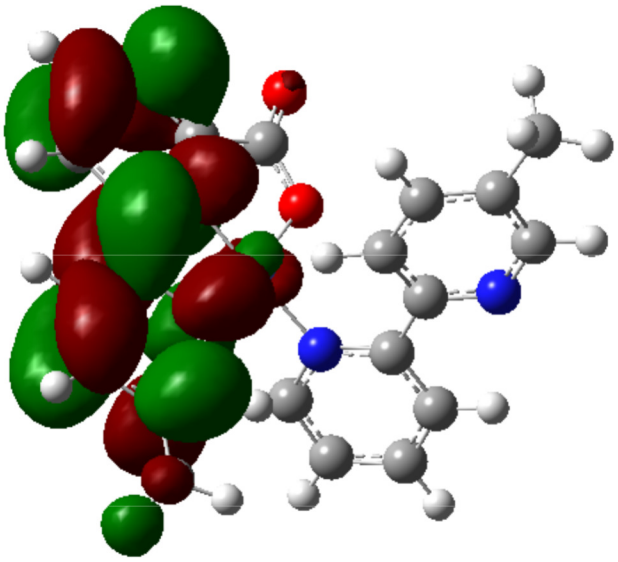

IV-LUMO

Fig. 3. Isodensity plots of the frontier orbitals of the complexes **I-IV**

are close to the reported results[26] although the absolute values are larger than that reported.

The other complexes have not been reported, we use the same method to study the tendency of the electronic structure. For compound **II** Ni(II)L_2, the pattern of occupied orbitals is qualitatively similar to that of the complex **I**. For the HOMO orbital, the largest orbital contributions arise from the metal atom (72 %) mixed with fewer characters of bipyridine rings (7-8 %) and carboxylic groups (6-7 %). But for the HOMO-1 and HOMO-2, the orbital contributions are mainly from the carboxylic groups (30-46 %), while for the HOMO-3 and HOMO-4, the orbital contributions are mainly from the bipyridine rings (27-37 %) and the carboxylic groups (10-19 %). The five lowest LUMOs of complex **II** is π* orbital's delocalized over the bipyridine ligands, over the range 29-90 %, with a little localization on the carboxylic groups, over the range 0-9 %. As this kind of sensitizers in photovoltaic solar cells anchor to TiO_2 semiconductor surface *via* acidic carboxylic or phosphoric units, it is commonly considered that large contribution from the carboxylic or phosphoric groups to the π* LUMOs, which associate with the final states in MLCT transitions, would favour the electron injection to TiO_2 conduction band quickly[26,47].

For compound **III** Mn(II)L_2 and compound **IV** Cu(II)L_2, the patterns of occupied orbitals are qualitatively different from that of complex **I**. In these two complexes, there are two single electrons, which are an α electron and β electron. In compound **III**, for the a electron, the HOMO of this complex is delocalized over on the carboxylic groups and a little on the bipyridine ligands, over the range 32-48 and 9-11 %, respectively, while for the β electron, the HOMO of this complex is delocalized over on the bipyridine rings, the metal atom and a little on the carboxylic groups, in the range of 47-48 %, 12 % and 1 %, respectively. For the HOMO-n (n = 1 - 4), the electron cloud delocalized over on the bipyridine rings and the carboxylic groups and the maximum percentage composition are 48 %. The six lowest LUMOs are π* orbital's delocalized over on the bipyridine ligands, ranging from 36-55 % and a little on the carboxylic groups, ranging from 1-7 %. In compound **IV**, for the α electron, the HOMO is delocalized over on the carboxylic groups and a little on the bipyridine ligands, over the range 7-87 and 5-7 %, respectively, while for the β electron, the HOMO is delocalized over on the bipyridine ligands and a little on the carboxylic groups, over the range 45-51 and 1 %, respectively. For the other HOMO-n (n = 1-4), the electron cloud delocalized over on the carboxylic groups. The six lowest LUMOs of both complexes are π* orbital's delocalized over the bipyridine ligands, over the range 3-92 % and 12-84 % for α and β electrons, respectively. In compound **III**, the electron transition forms are LLCT and MLCT, while in compound **IV**, which associate with the final states in LLCT transitions, M atoms only act as a bridge of LLCT transitions. The electron transition form of compound **IV** is different from those in compound **I**, **II** and **III**. In compound **III**, which associate with the final states in MLCT and LLCT transitions, the sensitizer would favour the electron injection to TiO_2 conduction band quickly[26,47]. However, there exists such a little contribution from the carboxylic groups to the π* LUMOs in the complex. It is attributed to the two carboxylic groups coordinating to the central Mn atom *via* two oxygen atoms, instead of being free to make a possible direct anchoring to TiO_2 surface just as that in the N3 and black dye[48,49]. So just as Falaras *et al*., showed, some reagent like HCl should be used to break Ru-O bonds and make carboxylic groups to adsorb on the TiO_2 surface[26].

Optical absorption spectrum: TDDFT//B3P86/LANL2DZ and TDDFT//B3P86/LANL2MB have been used to study the optical absorption spectra of organic metal compounds (Fig. 4). In order to inspect the method exactness, we selected the reported compound **I**[26] as a benchmark for comparison. Electronic excitation energies (wavelengths λ/nm), oscillator strengths f and the nature of the respective excited states (principal CI-coefficients) calculated by the TD-DFT method for all complexes were summarized in Table-3. Experimentally, the reported UV-visible maxima were found to be at 528 and 383 nm and a shoulder peak at 431 nm for the compound **I** (10^{-4} mol L^{-1} solution in DMF). However, the corresponding DFT values, based on B3LYP/LANL2DZ and

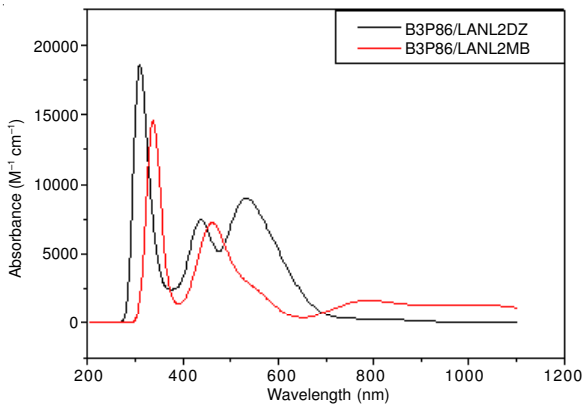

Calculated UV-visible spectra obtained for compounds **I**

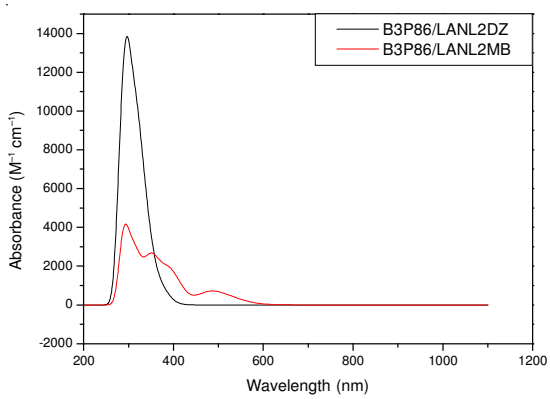

Calculated UV-visible spectra obtained for compounds **II**

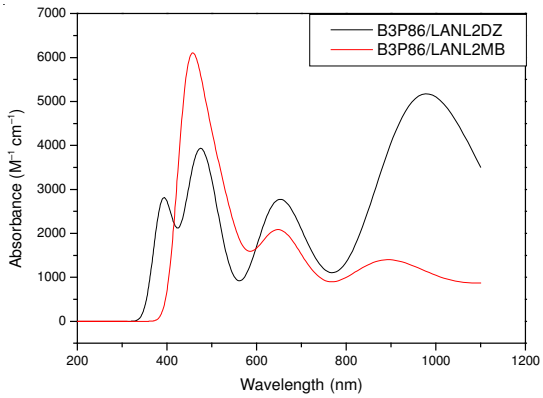

Calculated UV-visible spectra obtained for compounds **III**

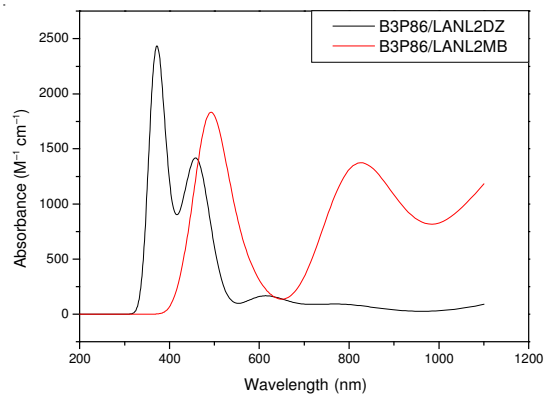

Calculated UV-visible spectra obtained for compounds **IV**

Fig. 4. Calculated UV-visible spectra obtained for compounds **I-IV** by the B3P86/LANL2DZ and B3P86/LANL2MB method

B3LYP/LANL2MB, are 203/244 and 341/460 nm, while the corresponding B3P86/LANL2DZ and B3P86/LANL2MB values are 307/432/530 and 334/456 nm, respectively. There are larger errors in the results using the B3LYP method compared with the experimental data. The values at 307, 432 and 530 nm from the B3P86/LANL2DZ method are in agreement with the reported absorption spectra[26]. This means that the outcomes based on the Becke-style 3-parameter density function theory using the Perdew86 correlation functional are more accurate than the outcomes based on the Becke-style 3-parameter density function theory using the Lee-Yang-Parr correlation functional. It is obvious that positions of the two band maximums in the observed spectrum are well reproduced in the simulated spectrum. However, the minimal wavelength and the relative intensity are not consistent well with the experimental data. Contrary to the experimental information, the simulated near-UV band is much higher than the visible one. The molar absorptive of the band maximum in visible region is slightly underestimated, while the one in the near-UV region is significantly overestimated. Similar results in simulation of N3-type dye also exist[50-52].

In compound **II** there is only one band maximum in the observed spectrum, while the corresponding DFT value, based on B3P86/LANL2DZ is at 321 nm. The transition form is mainly on the $HOMO_{-2}$-$LUMO_{+1}$ (14 %), $HOMO_{-3}$-LUMO (19 %), $HOMO_{-5}$-LUMO (18 %), $HOMO_{-6}$-LUMO (28 %). The all absorption peaks are in ultraviolet region. This means that the compound is not suitable as the dye-sensitized solar cell sensitizer.

In compound **III**, there are four band maxima in the observed spectrum, while the corresponding DFT values, based on B3P86/LANL2DZ and B3P86/LANL2MB, are 461/498/646/979 and 446/645/892 nm (Fig. 4), respectively. There are two single electrons in compound **III**, which are an α electron and β electron. The maximum absorption is in HOMO-LUMO of β-electron transition at 979 nm. At the 646 nm, the transition form is HOMO-$LUMO_{+2}$ of β electron transition. At the 498 nm, the contribution of the transition forms are complex, the main contribution are α electron transition in HOMO-LUMO, $HOMO_{-1}$-LUMO and a few of an β electron transition in HOMO-$LUMO_{+5}$. At the 461 nm, the contribution of the transition forms are more complex, the main contribution are a electron transition in $HOMO_{-1}$-LUMO, $HOMO_{-2}$-LUMO, $HOMO_{-4}$-$LUMO_{+1}$, $HOMO_{-6}$-$LUMO_{+3}$, $HOMO_{-8}$-$LUMO_{+1}$ and a few of an β electron transition in $HOMO_{-4}$-$LUMO_{+1}$, $HOMO_{-5}$-LUMO, $HOMO_{-7}$-LUMO, $HOMO_{-8}$-$LUMO_{+1}$. From the above analysis of the contribution to the HOMOs and LUMOs (Table-2), the transition form is attributed to the LLCT with a few MLCT. The absorption peaks are all in visible region, the λ_{max} band in complex **III** has a large red-shift when compared to the standard compound **I**. This means that the panchromatic response of compound **III** renders it as a suitable sensitizer for solar energy conversion applications.

In compound **IV**, there are three band maxima in the observed spectrum, while the corresponding DFT values, based on B3P86/LANL2DZ and B3P86/LANL2MB, are 379/462/617 and 492/822/824 nm, (Fig. 4), respectively. There are also two single electrons in this compound, which are α and β electrons. There are many transitions with small oscillator

TABLE-3
ELECTRONIC EXCITATION ENERGIES (WAVELENGTHS λ/nm), OSCILLATOR STRENGTHS f AND NATURE OF THE RESPECTIVE EXCITED STATE (PRINCIPAL CI-COEFFICIENTS) CALCULATED BY THE TDDFT METHOD FOR ALL COMPOUNDS

Comp.	B3LYP/LANL2DZ				B3LYP/LANL2MB			
	λ (nm)	f	CI	Main configurations	λ (nm)	f	CI	Main configurations
I	246	0.4976	0.4770	HOMO-LUMO	1036.99	0.0176	0.6695	HOMO-LUMO
	231	0.0669	0.2860	$HOMO_{-7}$-$LUMO_{+2}$	779.81	0.0219	0.6753	$HOMO_{-1}$-LUMO
	221	0.0288	0.3099	$HOMO_{-1}$-$LUMO_{+2}$	555.76	0.0249	0.6603	HOMO-$LUMO_{+2}$
	212	0.0567	0.3709	$HOMO_{-1}$-$LUMO_{+5}$	473.83	0.0235	0.5115	$HOMO_{-1}$-$LUMO_{+2}$
	204	0.4429	0.3521	$HOMO_{-2}$-LUMO	460.03	0.0507	0.5524	$HOMO_{-6}$-LUMO
II	391	0.0035	0.59285	HOMO-LUMO	513	0.0047	0.8552	HOMO-LUMO
	236	0.0958	0.31101	$HOMO_{-11}$-LUMO	476	0.0069	0.6406	$HOMO_{-1}$-LUMO
	233	0.6202	0.31962	$HOMO_{-1}$-LUMO	385	0.0166	0.4235	$HOMO_{-1}$-$LUMO_{+3}$
	220	0.1522	0.23424	HOMO-$LUMO_{+2}$	355	0.0187	0.3535	$HOMO_{-4}$-$LUMO_{+1}$
	219	0.0637	0.25196	$HOMO_{-7}$-$LUMO_{+6}$	326	0.0209	0.4973	HOMO-$LUMO_{+5}$
	218	0.0014	0.26800	$HOMO_{-1}$-$LUMO_{+2}$	310	0.0191	0.3678	HOMO-$LUMO_{+5}$
	210	0.0013	0.38931	$HOMO_{-1}$-$LUMO_{+6}$	298	0.0191	0.4037	$HOMO_{-1}$-$LUMO_{+5}$
	210	0.0271	0.38155	HOMO-$LUMO_{+6}$	296	0.0077	0.4653	$HOMO_{-1}$-$LUMO_{+5}$
	200	0.0079	0.27696	$HOMO_{-5}$-$LUMO_{+2}$	284	0.0141	0.5264	$HOMO_{-6}$-LUMO
III	882	0.0639	0.9640	HOMO-LUMO	1291	0.0165	0.9467	HOMO-LUMO
	605	0.0254	0.9779	$HOMO_{-1}$-LUMO	881	0.0184	0.9301	HOMO-$LUMO_{(\alpha)}$
	504	0.0349	0.9611	HOMO-$LUMO_{+2}$	633	0.0152	0.9112	$HOMO_{-1}$-LUMO
	485	0.0093	0.9865	HOMO-$LUMO_{(\alpha)}$	541	0.0129	0.6408	HOMO-$LUMO_{+2(\alpha)}$
	465	0.0206	0.8831	$HOMO_{-1}$-$LUMO_{+2}$	506	0.0167	0.5941	H_{-2}-$LUMO_{+2(\alpha)}$
	412	0.0055	0.4306	$HOMO_{-1}$- $LUMO_{(\alpha)}$	468	0.0139	0.4377	H_{-1}-$LUMO_{+2(\alpha)}$
	403	0.0151	0.7726	HOMO-$LUMO_{+5(\alpha)}$	451	0.0364	0.4988	HOMO-$LUMO_{+5(\alpha)}$
IV	1381	0.0039	0.7080	HOMO-LUMO	1010	0.0247	0.5388	HOMO-LUMO
	477	0.0052	0.5979	$HOMO_{-2}$-LUMO	705	0.0093	0.9774	HOMO-$LUMO_{+1}$
	470	0.0047	0.8244	$HOMO_{-1}$-LUMO	616	0.0046	0.9760	HOMO-$LUMO_{+2}$
	456	0.0049	0.8767	HOMO-$LUMO_{+2}$	553	0.0065	0.4669	$HOMO_{-1}$-$LUMO_{+1}$
	370	0.0057	0.4662	$HOMO_{-3}$-$LUMO_{(\alpha)}$	542	0.0069	0.5018	$HOMO_{-1}$-$LUMO_{(\alpha)}$
	–	–	–	–	526	0.0047	0.5646	HOMO-$LUMO_{(\alpha)}$
	–	–	–	–	510	0.0088	0.5272	HOMO-$LUMO_{+3}$
Comp.	B3P86/ LANL2DZ				B3P86/ LANL2MB			
	λ (nm)	f	CI	Main configurations	λ (nm)	f	CI	Main configurations
I	594	0.0528	0.5966	$HOMO_{-1}$-LUMO	781	0.0221	0.6736	$HOMO_{-1}$-LUMO
	522	0.1000	0.5466	HOMO-$LUMO_{+2}$	552	0.0256	0.6568	HOMO-$LUMO_{+2}$
	442	0.0588	0.6166	$HOMO_{-1}$-LUMO	471	0.0226	0.4912	$HOMO_{-1}$-$LUMO_{+2}$
	432	0.0392	0.6354	HOMO-$LUMO_{+4}$	455	0.0566	0.5671	$HOMO_{-7}$-LUMO
	328	0.0611	0.5857	$HOMO_{-6}$-LUMO	341	0.0156	0.5589	$HOMO_{-3}$-$LUMO_{+3}$
	319	0.0357	0.6455	HOMO-$LUMO_{+6}$	337	0.1487	0.4646	$HOMO_{-7}$-LUMO
	311	0.0224	0.6372	$HOMO_{-5}$-$LUMO_{+1}$	333	0.0135	0.5261	$HOMO_{-3}$-$LUMO_{+5}$
	305	0.1965	0.5621	$HOMO_{-9}$-LUMO	331	0.0213	0.4970	$HOMO_{-6}$-$LUMO_{+2}$
II	344	0.0290	0.4566	$HOMO_{-3}$-LUMO	478	0.0081	0.6448	$HOMO_{-1}$-LUMO
	333	0.0209	0.4303	$HOMO_{-5}$-LUMO	401	0.0070	0.4557	$HOMO_{-3}$-$LUMO_{+1}$
	321	0.0474	0.3510	$HOMO_{-6}$-LUMO	386	0.0130	0.4059	$HOMO_{-1}$-$LUMO_{+3}$
	316	0.0380	0.5290	$HOMO_{-2}$-$LUMO_{+1}$	350	0.0165	0.5291	$HOMO_{-3}$-$LUMO_{+2}$
	300	0.0410	0.4940	$HOMO_{-8}$-LUMO	347	0.0071	0.4013	$HOMO_{-4}$-$LUMO_{+1}$
	296	0.0332	0.5768	$HOMO_{-4}$-$LUMO_{+2}$	322	0.0165	0.6032	HOMO-$LUMO_{+5}$
	292	0.0379	0.4922	$HOMO_{-7}$-$LUMO_{+1}$	307	0.0184	0.4207	$HOMO_{-4}$-$LUMO_{+4}$
	290	0.0387	0.4127	$HOMO_{-3}$-$LUMO_{+3}$	291	0.0356	0.3576	$HOMO_{-4}$-$LUMO_{+2}$
	279	0.0501	0.3498	$HOMO_{-3}$-$LUMO_{+3}$	284	0.0145	0.2442	$HOMO_{-2}$-$LUMO_{+6}$
III	979	0.0714	0.9529	HOMO-LUMO	1327	0.0153	0.9439	HOMO-LUMO
	691	0.0074	0.9910	$HOMO_{-1}$-LUMO	892	0.0189	0.9219	HOMO-$LUMO_{(\alpha)}$
	646	0.0326	0.9813	HOMO-$LUMO_{+2}$	645	0.0202	0.8692	$HOMO_{-1}$-LUMO
	498	0.0206	0.9174	HOMO-$LUMO_{(\alpha)}$	537	0.0152	0.6276	HOMO-$LUMO_{+2(\alpha)}$
	476	0.0053	0.6591	$HOMO_{-1}$-$LUMO_{+2}$	506	0.0180	0.5539	H_{-2}-$LUMO_{+2(\alpha)}$
	461	0.0329	0.8265	$HOMO_{-1}$- $LUMO_{(\alpha)}$	468	0.0173	0.4352	H_{-1}-$LUMO_{+2(\alpha)}$
	–	–	–	–	446	0.0322	0.6825	HOMO-$LUMO_{+5(\alpha)}$
IV	1390	0.0036	0.7277	HOMO-LUMO	1216	0.0171	0.8535	$HOMO_{-2}$-LUMO
	464	0.0036	0.8417	$HOMO_{-4}$-LUMO	824	0.0135	0.9757	HOMO-$LUMO_{+1}$
	462	0.0072	0.5998	$HOMO_{-2}$-LUMO	822	0.0053	0.9807	HOMO-$LUMO_{+2}$
	417	0.0028	0.6275	HOMO-$LUMO_{(\alpha)}$	472	0.0034	0.9792	HOMO-$LUMO_{+6}$
	379	0.0041	0.3089	$HOMO_{-2}$-$L_{+1(\alpha)}$	435	0.0023	0.6292	$HOMO_{-1}$-$L_{+2(\alpha)}$

strength obtained in this compound. At 617 nm, the transition forms are $HOMO_{-2}$-LUMO (10 %), $HOMO_{-8}$-LUMO (19 %) and $HOMO_{-10}$- LUMO (13 %) of β electron transition. At the 462 nm, the transition form is HOMO-$LUMO_{+2}$ (17 %), HOMO-LUMO (19 %), $HOMO_{-2}$-LUMO (38 %) and $HOMO_{-4}$-LUMO (24 %) of β electron transition and HOMO-LUMO (1 %) of α electron transition. At the 379 nm, the transition form is $HOMO_{-1}$-$LUMO_{+2}$ (7 %), $HOMO_{-2}$-$LUMO_{+1}$ (10 %) and $HOMO_{-3}$-$LUMO_{+2}$ (23 %), of β electron transition and $HOMO_{-1}$-$LUMO_{+1}$ (4 %), $HOMO_{-2}$-$LUMO_{+1}$ (11 %) and $HOMO_{-3}$-$LUMO_{+1}$ (4 %) of α electron transition. From the above analysis of the contribution to the HOMOs and LUMOs (Table-2), more molecular orbitals contribute to those transitions of complex and the transition form is attributed to the LLCT. The absorption peaks are all in visible region and the λ_{max} band in complex **IV** has a large red-shift when compared to the standard compound **I**. This means that the compound **IV** is also a suitable replacement as the dye-sensitized solar cell sensitizer.

Conclusion

In this paper, DFT methods have been used to study some organic-metal compounds. The geometry, electronic structure and optical absorption spectra of these organic-metal compounds have been investigated by means of combined DFT/TD-DFT calculations. Frontier orbital analysis shows different contributions of the HOMOs and LUMOs. In compounds **I** and **II**, the HOMOs are mainly on the metal atoms, the LUMOs are mainly on the bipyridine rings. This means that the electron transition is attributed to the MLCT. In compounds **III** and **IV**, the HOMOs are mainly on the bipyridine rings and carboxylic groups, the LUMOs are mainly on the bipyridine rings and a few on the carboxylic groups. There is only an oxygen atom of the carboxylic groups coordinating to the central metal atom. This made the other oxygen atom of the carboxylic groups to make a possible directed anchoring to TiO_2 surface. The calculated absorption spectra (based on B3P86/LANL2DZ) are in excellent agreement with the experimental data of compound **I**. The same method was used to predict the other compounds. The compounds **III** and **IV** show panchromatic response. The analysis of these compounds about the optical absorption spectra shows that the absorption peaks are all in visible region and the lmax bands in complexes **III** and **IV** have a large red-shift when compared to the standard compound **I**. Indicating that compound **III** and **IV** are suitable replacement as the dye-sensitized solar cell sensitizer. The normal transition metals to replace the noble metal will decrease cost of the dye-sensitized solar cells.

ACKNOWLEDGEMENTS

This work was supported by the Jiangsu Postdoctoral Foundation (Grant No. 1001010c) and the funds from Jiangsu Province Education Office (Serial No.: JH10-48).

REFERENCES

1. B. Oregan and M. Grätzel, *Nature*, **353**, 737 (1991).
2. M. Grätzel, *Nature*, **414**, 338 (2001).
3. A. Hagfeldt and M. Grätzel, *Acc. Chem. Res*., **33**, 269 (2000).
4. M. Grätzel, *J. Photochem. Photobiol. C*, **4**, 145 (2003).
5. S. Wang, Z.C. Yu, L. Han, C.L. Dai and J.Y. Song, *Asian J. Chem.*, **24**, 214 (2012).
6. S. Altobello, R. Argazzi, S. Caramori, C. Contado, S.D. Fré, P. Rubino, C. Choné, G. Larramona and C.A. Bignozzi, *J. Am. Chem. Soc*., **127**, 15342 (2005).
7. T. Yoshida, J. Zhang, D. Komatsu, S. Sawatani, H. Minoura, T. Pauporté, D. Lincot, T. Oekermann, D. Schlettwein, H. Tada, D. Wöhrle, K. Funabiki, M. Matsui, H. Miura and H. Yanagi, *Adv. Funct. Mater*., **19**, 17 (2009).
8. F. Odobel, L.L. Pleux, Y. Pellegrin and E. Blart, *Acc. Chem. Res*., **43**, 1063 (2010).
9. Y. Wang, Y. Liu, H. Yang, H. Wang, H. Shen and M. Li and J. Yan, *Curr. Appl. Phys*., **10**, 119 (2010).
10. V.M. Guérin, C. Magne, T. Pauporté, T.L. Bahers and J. Rathousky, *ACS Appl. Mater. Interf.*, **2**, 3677 (2010).
11. S.E. Koops, B.C. O'Regan, P.R.F. Barnes and J.R. Durrant, *J. Am. Chem. Soc*., **131**, 4808 (2009).
12. H.X. Wang, H. Li, B.F. Xue, Z.X. Wang, Q.B. Meng and L.Q. Chen, *J. Am. Chem. Soc*., **127**, 6394 (2005).
13. B.F. Xue, Z.W. Fu, H. Li, X.Z. Liu, S.C. Cheng, J. Yao, D.M. Li, L.Q. Chen and Q.B. Meng, *J. Am. Chem. Soc*., **128**, 8720 (2006).
14. M.K. Nazeeruddin, A. Kay, I. Rodicio, R. Humphry-Baker, E. Müller, P. Liska, N. Vlachopoulos and M. Grätzel, *J. Am. Chem. Soc*., **115**, 6382 (1993).
15. M.K. Nazeeruddin, P. Pèchy, T. Renouard, S.M. Zakeeruddin, R. Humphry-Baker, P. Comte, P. Liska, L. Cevey, E. Costa, V. Shklover, L. Spiccia, G.B. Deacon, C.A. Bignozzi and M. Grätzel, *J. Am. Chem. Soc*., **123**, 1613 (2001).
16. J.J. Lagref, M.K. Nazeeruddin and M. Grätzel, *Synth. Met*., **138**, 333 (2003).
17. Y.N. Park, Y.M. Jung, S. Sarker, J.J. Lee, Y.H. Lee, K.T. Lee, J.J. Oh and S.W. Joo, *Sol. Energy Mater. Sol. Cells*, **94**, 857 (2010).
18. J.M. Villegas, S.R. Stoyanov, W. Huang, L.L. Lockyear, J.H. Reibenspies and D.P. Rillema, *Inorg. Chem*., **43**, 6383 (2004).
19. A. Mishra, M.K.R. Fischer and P. Bäuerle, *Angew. Chem. Int. Ed*., **48**, 2474 (2009).
20. S. Altobello, R. Argazzi, S. Caramori, C. Contado, S.D. Fré, P. Rubino, C. Choné, G. Larramona and C.A. Bignozzi, *J. Am. Chem. Soc*., **127**, 15342 (2005).
21. M.K. Nazeeruddin, F. De Angelis, S. Fantacci, A. Selloni, G. Viscardi, P. Liska, S. Ito, B. Takeru and M. Grätzel, *J. Am. Chem. Soc*., **127**, 16835 (2005).
22. Y. Chiba, A. Islam, Y.Watanabe, R. Komiya, N. Koide and L. Han, *J. Appl. Phys. (Japan)*, **45**, 638 (2006).
23. M.K. Nazeeruddin, T. Bessho, L. Cevey, S. Ito, C. Klein, F. De Angelis, S. Fantacci, P. Comte, P. Liska, H. Imai and M. Grätzel, *J. Photochem. Photobiol. A*, **185**, 331 (2007).
24. F. Gao, Y. Wang, J. Zhang, D. Shi, M. Wang, R. Humphry-Baker, P. Wang, S.M. Zakeeruddin and M. Grätzel, *Chem. Commun*., 2635 (2008).
25. N.O. Komatsuzaki, M. Yanagida, T. Funaki, K. Kasuga, K. Sayama and H. Sugihara, *Sol. Energy Mater. Sol. Cells*, **95**, 310 (2011).
26. Y. Xu, W.K. Chen, M.J. Cao, Sh. H. Liu, J.Q. Li, A.I. Philippopoulos and P. Falaras, *Chem. Phys*., **330**, 204 (2006).
27. C. Barolo, M.K. Nazeeruddin, S. Fantacci, D.D. Censo, P. Comte, P. Liska, G. Viscardi, P. Quagliotto, F. D. Angelis, S. Ito and M. Grätzel, *Inorg. Chem*., **45**, 4642 (2006).
28. A.I. Philippopoulos, E. Chatzivasiloglou, A. Terzis, T.P. Raptopoulou, P. Tisnès, C. Picard and P. Falaras, *Inorg. Chem. Commun*., **8**, 162 (2005).
29. S. Sagdinc and H. Pir, *Spectrochim. Acta A*, **73**, 181 (2009).
30. P.S. Liyanage, R.M. de Sliva and K.M.N. de Sliva, *J. Mol. Struct. (Theochem.)*, **639**, 195 (2003).
31. F.D. Angelis, S. Fantacci, A. Selloni and M.K. Nazeeruddin, *Chem. Phys. Lett*., **415**, 115 (2005).
32. A. Islam, F.A. Chowdhury, Y. Chiba, R. Komiya, N. Fuke, N. Ikeda, K. Nozaki and L.Y. Han, *Chem. Mater*., **18**, 5178 (2006).
33. T. Bessho, E. Yoneda, J.H. Yum, M. Guglielmi, I. Tavernelli, H. Imai, U. Rothlisberger, M.K. Nazeeruddin and M. Grätzel, *J. Am. Chem. Soc*., **131**, 5930 (2009).
34. F. Aiga and T. Tada, *Sol. Energy Mater. Sol. Cells*, **85**, 437 (2005).
35. T.H. Dunning Jr. and P.J. Hay, In ed.: H.F. Schaefer III, In Modern Theoretical Chemistry, Plenum, New York, Vol. 3, No. 1 (1976).
36. P.J. Hay and W.R. Wadt, *J. Chem. Phys*., **82**, 270 (1985).
37. W.R. Wadt and P.J. Hay, *J. Chem. Phys*., **82**, 284 (1985).
38. P.J. Hay and W.R. Wadt, *J. Chem. Phys*., **82**, 299 (1985).
39. W.J. Hehre, R.F. Stewart and J.A. Pople, *J. Chem. Phys*., **51**, 2657 (1969).

40. J.B. Collins, P.V.R. Schleyer, J.S. Binkley and J.A. Pople, *J. Chem. Phys*., **64**, 5142 (1976).
41. HyperChem Pro. Release 6.03, Hypercube Inc., USA (2004).
42. S.M. Couchman, J.C. Jeffery and M.D. Ward, *Polyhedron*, **18**, 2633 (1999).
43. P. Segla, D. Milkoš, P. Olejníková, B. Kalináková, D. Hudecová, M. Palicová, J. Švorec, M. Valko, M. Melník and T. Glowiak, *Inorg. Chim. Acta*, **357**, 4172 (2004).
44. M. Devereux, M. McCann, V. Leon, V. McKee and R.J. Ball, *Polyhedron*, **21**, 1063 (2002).
45. E. Garribba, G. Micera and M. Zema, *Inorg. Chim. Acta*, **357**, 2038 (2004).
46. M.J. Plater, M.R.S.J. Foreman, J.M.S. Skakle and R.A. Howie, *Inorg. Chim. Acta*, **332**, 135 (2002).
47. S. Fantacci, F.D. Angelis and A. Selloni, *J. Am. Chem. Soc*., **125**, 4381 (2003).
48. M.K. Nazeeruddin, A. Kay, I. Rodicio, R.H. Baker, E. Müller, P. Liska, N. Vlachopoulos and M. Grätzel, *J. Am. Chem. Soc*., **115**, 6382 (1993).
49. M.K. Nazeeruddin, P. Pèchy, T. Renouard, S.M. Zakeeruddin, R.H. Baker, P. Comte, P. Liska, L. Cevey, E. Costa, V. Shklover, L. Spiccia, G.B. Deacon, C.A. Bignozzi and M. Grätzel, *J. Am. Chem. Soc*., **123**, 1613 (2001).
50. J.E. Monat, J.H. Rodriguez and J.K. Mccusker, *J. Phys. Chem. A*, **106**, 7399 (2002).
51. F.D. Angelis, S. Fantacci, A. Selloni and M.K. Nazeeruddin, *Chem. Phys. Lett*., **415**, 115 (2005).
52. F.D. Angelis, S. Fantacci and A. Selloni, *Chem. Phys. Lett*., **389**, 204 (2004).